International Journal of Nanomedicine

Dovepress
open access to scientific and medical research

Open Access Full Text Article

ORIGINAL RESEARCH

Dual micelles-loaded gelatin nanofibers and their application in lipopolysaccharide-induced periodontal disease

This article was published in the following Dove Medical Press journal:
International Journal of Nanomedicine

Yabing Wang[1]
Haoxuan Li[2]
Yanhuizhi Feng[3]
Peilin Jiang[2]
Jiansheng Su[1]
Chen Huang[2]

[1]Department of Prosthodontics, School & Hospital of Stomatology, Tongji University, Shanghai Engineering Research Center of Tooth Restoration and Regeneration, Shanghai 200072, China; [2]Key Laboratory of Textile Science & Technology, Ministry of Education, College of Textiles, Donghua University, Shanghai 201620, China; [3]Department of Periodontics, School & Hospital of Stomatology, Tongji University, Shanghai Engineering Research Center of Tooth Restoration and Regeneration, Shanghai 200072, China

Introduction: Combined therapies utilizing inhibitors to remove pathogens are needed to suppress lipopolysaccharide (LPS)-induced periodontal disease. We prepared a novel, multi-agent delivery scaffold for periodontal treatment.

Methods: In this study, we synthesized SP600125 (a JNK inhibitor) and SB203580 (a p38 inhibitor) drug-loaded poly(ethylene glycol)-block-caprolactone copolymer via dialysis method. The physical property of micelles was characterized through dynamic light scattering and transmission electron microscopy. The cell growth and LPS-induced MMP-2 and MMP-13 expression were evaluated through CCK-8, real-time PCR and Western blot assay. The release of SP600125 and SB203580 from different scaffolds was estimated. Microcomputed tomography and histology were used for evaluating the effect of the micelles-loaded nanofibers on the treatment of class II furcation defects in dogs.

Results: The drug was then successfully incorporated into gelatin fibers during electrospinning process. We confirmed that the micelles had spherical structure and an average particle size of 160 nm for SP600125-micelles (SP-Ms) and 150 nm for SB203580-micelles (SB-Ms). The nanofiber scaffold showed excellent encapsulation capability, in vitro drug-release behavior, and cell compatibility. Real-time PCR and Western blot assay further indicated that LPS-induced MMP-2 and MMP-13 expression was significantly inhibited by the scaffold.

Conclusion: The results suggested that the dual drug-loaded system developed in this study might become a highly effective therapy for periodontal disease.

Keywords: periodontal disease, controlled release, drug-loaded micelles, electrospun nanofibers, scaffold

Correspondence: Jiansheng Su
Department of Prosthodontics, School & Hospital of Stomatology, Tongji University, Shanghai Engineering Research Center of Tooth Restoration and Regeneration, YanChangZhong Road 399, Shanghai 200072, China
Tel +86 21 5672 2215
Fax +86 21 6652 4025
Email sjs@tongji.edu.cn

Chen Huang
Key Laboratory of Textile Science & Technology, Ministry of Education, College of Textiles, Donghua University, RenMingBei Road 2999, Shanghai 201620, China
Tel +86 21 6779 2741
Fax +86 21 6779 2743
Email hc@dhu.edu.cn

Introduction

Periodontal disease is the major cause of destruction of osseous and surrounding soft tissues, which is currently treated through ultrasonic scaling and root planning.[1] However, as pathogens cannot be completely removed in these treatments, soft tissue and other anatomically inaccessible areas (eg, furcation and root depressions) are vulnerable to infection.[2] Therefore, combined therapies utilizing inhibitors to remove pathogens are needed to suppress lipopolysaccharide (LPS)-induced periodontal disease.

Recent research has shown that blocking the formation of reactive matrix metalloproteinases (MMPs) by inhibitors may be an effective approach to treat periodontitis complications.[3] Attribution to the understanding that MMPs derived from periodontal cells are a group of neutral endopeptidases, such as interstitial collagenase, gelatinases, stromelysin, matrilysin, metalloelastase, and membrane-type MMPs,[4,5] which play key roles in destructing periodontal tissue.[6] In particular, MMP-2 is considered as the major culprit in the breakdown of periodontal tissues[7] and is also the main proteolytic

submit your manuscript | www.dovepress.com
Dovepress
http://dx.doi.org/10.2147/IJN.S182073

enzyme that cleaves collagen I, III, IV, gelatin, elastin, and fibronectin,[8] whilst MMP-13 is associated with the destructive periodontal disease in humans.[9]

SP600125 and SB203580 are c-Jun N-terminal kinase (JNK) and p38 MAP (P38) kinase inhibitors that belong to mitogen-activated protein kinase families. The JNK pathway has been shown to be involved in MMP-1 and MMP-3 expression in periodontal ligament (PDL) cells,[10] and the P38 pathway is involved in transcription of MMP-13 by LPS-induced periodontal pathogenicity.[11] However, the inhibition of these pathways suffers from inherent limitation in that most of the inhibitors are insoluble in water, making it difficult for majority of the inhibitors to be released sustainably in oral cavity. Furthermore, it is hard to disperse and encapsulate drugs owing to the immiscible nature of these drugs in aqueous solutions, which greatly weakens their effects in diseases and wounds that involve moisture environments. The hydrophobic core of micelles provides an adjustable loading space for water-insoluble drugs, which effectively improved their bioavailability by increasing the solubility.[12] In addition, due to their small particle size, micelles are able to penetrate into the alveolar bone trabeculae, the connective tissue, and even the periodontal pocket areas underneath the gum, which may significantly improve the antibacterial effect.[13] Furthermore, polymeric micelles possess some advantages, such as largely enhanced drug solution in water, sustained release, prolonged circulation, tumor localization by enhanced permeability and retention effect, and decreased side effects.[14] However, in the periodontal environment, it is difficult for the polymeric micelles to be released in a controlled manner. For example, in the treatment of infection and pain after surgical procedure, the release of two or more different drugs cannot be controlled at proper time or in appropriate doses.[15]

There are many different membranes that are used for guided tissue regeneration treatment in humans and these have been evaluated in dogs. They include poly-L-lactic acid, collagen, expanded polytetrafluoroethylene, and lactic acid-glycolic acid copolymer.[16–19] However, these materials are strictly used as physical barriers to avoid soft tissue ingress to periodontal defects. Electrospun nanofibers constitute another major type of materials used in biomedical field, mainly because they can mimic the native extracellular matrix (ECM) both topographically and compositionally.[20,21] One specific example for periodontal application is by electrospinning process, Macro et al prepared a spatially designed and multi-functional nanofiber membrane that could promote periodontal regeneration.[22] Nevertheless, current study on electrospun scaffolds for periodontal regeneration mainly focuses on structural modification by different functional layers or facilitating tissue growth by introducing growth factors and other water-soluble biological molecules.[23,24] None of these studies has tried to suppress inflammatory oral diseases by inhibiting the expression and activity of MMPs. Given the need for regenerative therapy of periodontal defects, we developed a new scaffold that combines micelles with MMP inhibitors and electrospun nanofibers. We hypothesize that such systems might be used to achieve the sustained release of MMP inhibitors (MMPIs) and subsequent long-term blockage of MMP in periodontal diseases.

To validate this assumption, herein we developed a two-step method to prepare micelle-enriched electrospun nanofiber scaffolds. The mitogen-activated protein kinase inhibitors, SP600125 and SB203580, were loaded into poly(ethylene glycol)-block-poly(ε-caprolactone) (mPEG-PCL) micelles, which allowed us to evenly incorporate the micelles into nanofibers by electrospinning of gelatin aqueous solution. Physiochemical assessments suggest that the drugs can be released for a long term. The excellent healing effects of the scaffold were demonstrated via both in vitro cell compatibility and in vivo periodontal wound healing of class II furcation defects in beagle dogs. These results make us believe that the combination of polymeric micelles and electrospun nanofibers may become a universal methodology for the incorporation and the release of water-insoluble drugs.

Materials and methods

Materials

Poly(ethylene glycol)$_{2000}$-block- caprolactone$_{2000}$ (mPEG$_{2000}$-PCL$_{2000}$) was purchased from Jinan DaiGang Biomaterials Company (Shangdong, China). Amine PEG polycaprolactone block copolymer, PEG (NH_2-PEG$_{2000}$-b-PCL$_{2000}$), was supplied by JenKem Technology Co., Ltd. (Beijing, China). SP600125 and SB203580 were purchased from Selleckchem (Houston, TX, USA). Antibodies to the fibroblast protein marker vimentin (ab8978), epithelial protein maker cytokeratin (ab181598), human fibroblast MMP-2 protein (ab37150) and MMP-13 protein (ab39012) were obtained from Abcam (Cambridge, UK). Cell proliferation was evaluated with Cell Counting Kit-8 (CCK-8) from Dojindo (Kumamoto, Japan). DMEM, gimethylformamide (DMF), and FBS were purchased from Sigma-Aldrich Co. (St Louis, MO, USA). 1-(3-Dimethylaminopropyl)-3-ethylcarbodiimide hydrochloride (EDC; Sigma-Aldrich Co.) and N-hydroxysulfosuccinimide (NHS; Pierce Chemicals, Dallas, TX, USA) were used as cross-linking agents for gelatin nanofibers.

Preparation of SP600125/SB203580-loaded micelles

Micelles containing SP600125 and SB203580 were prepared as follows. Twenty milligrams of poly(ethylene

glycol)-block-polycaprolactone (PEG-b-PCL) and SP600125 or SB203580 (0.32 mg, Selleckchem) were firstly dissolved in DMF. MilliQ water was then added dropwise under continuous stirring, and the suspension was dialyzed (Spectra/Por membrane MWCO: 8,000) against water (which was changed at least eight times) for 24 hours. The acquired micelles were sterile-filtered with a 13 mm syring filter (0.2 μm; EMD Millipore, Billerica, MA, USA) and freeze-dried. Labeled micelles (20 mg) containing SP600125 (0.32 mg) or SB203580 (0.32 mg) were prepared by dissolving the $mPEG_{2000}$-PCL_{2000} and NH_2-PEG_{2000}-b-PCL_{2000} (90/10) in 0.1 mg/mL Alexa Fluor® 488 NHS Ester or Alexa Fluor 647 NHS Ester (succinimidyl ester) solution (Thermo Fisher Scientific, Waltham, MA, USA), and then the suspension was dialyzed (Spectra/Por membrane MWCO: 8,000) against water.

Morphology and particle size

Particle size of micelles was determined by dynamic light scattering with a Nano-Zs Malvern Nano analyzer (Malvern Instruments, Malvern, UK). The data from five measurements were averaged to obtain the mean particle size. Micelle morphology was observed under an H-600 transmission electron microscope (TEM; Hitachi, Tokyo, Japan), with a drop of PEG-b-PCL micelle solution (1.0 mg/mL in water) placed on a grid coated with Formvar and carbon film and air-dried at room temperature.

Drug entrapment efficiency and loading capacity

The freeze-dried micelles were dissolved in DMF and placed under ultrasonic treatment for 2 hours. The drug concentrations in the supernatant were then analyzed with an ultraviolet-visible spectrophotometer (Optizen 3220; Mecasys, Daejeon, Korea) at the highest wavelengths (301 nm and 313 nm). We then constructed a standard calibration curve to represent different concentrations of SP600125 and SB203580 (0.01–50 μg) vs maximum absorbance. All experiments were performed in triplicate as reported to ensure reproducibility. The encapsulation efficiency (EE) and loading capacity (LC) of the micelles were determined according to Equations 1 and 2, respectively.

$$EE\,(\%) = \left(\frac{\text{Amount of loaded drug}}{\text{Amount of feeding drug}}\right) \times 100 \quad (1)$$

$$LC\,(\%) = \left(\frac{\text{Amount of loaded drug}}{\text{Amount of drug-loaded micelle}}\right) \times 100\% \quad (2)$$

Table 1 Composition of mixtures used for film preparation (w/v%)

Ingredients	S0	S1	S2	S3
SP600125-loaded micelles	0%	8%	0%	4%
SB203580-loaded micelles	0%	0%	8%	4%
Gelatin	60%	60%	60%	60%

Note: The suspension containing 8% drug-loaded micelles into a 60 w/v% gelatin solution (S) obtained by dissolving 1.5 g gelatin into 2.5 mL of deionized water shows a uniform particle distribution without aggregation.

Electrospinning

Ratios of polymers in the solution blend are listed in Table 1. Gelatin (120%, w/v) was dissolved in 1 mL of deionized (DI) water at 60°C. After dissolving the gelatin, another 1 mL of DI water with different amounts of micelle powder was added into the solution, and each mixture was vigorously stirred at room temperature until it became homogeneous. The electrospinning process is illustrated in Figure 1A. The blended solution was loaded into a 5 mL plastic syringe connected to a stainless needle (inner diameter =0.7 mm). The syringe was fixed horizontally on a microinjection pump (LSP02-1B; Longer Pump, Beijing, China), and an aluminum foil-coated plate was placed 14 cm away from the tip of the needle. All blended solutions and the pure gelatin solution were electrospun at 15 kV under a flow rate of 0.5 $mL{\cdot}h^{-1}$. The electrospun fibers containing labeled micelles were collected in darkness at room temperature. As listed in Table 1, the final solution blends were pure gelatin fibers (S0), SP600125-Ms-loaded fibers (S1), SB203580-Ms-loaded fibers (S2), and SP600125-Ms/SB203580-Ms-loaded fibers (S3).

Characterization of the fibrous scaffold

The morphology of the samples was investigated by a scanning electron microscope (SEM) (JSM-7001F; JEOL, Tokyo, Japan). All samples were sputtered with platinum film prior to observation. The labeled SP600125-Ms/SB203580-Ms nanofibers were collected on glass slides and stored in darkness until observation. The ImageJ software was used to determine diameters of nanofiber based on SEM images of six randomly selected areas of the nanofibers. Confocal laser scanning microcopy (CLSM, Olympus FV1000) was applied to visualize SP-Ms/SB-Ms inside the nanofibers, where Alexa Fluor 488 NHS Ester and Alexa Fluor 647 NHS Ester were excited at 494 and 651 nm, respectively.

In vitro drug release study

All samples were pretreated as follows before drug release and cell culture analyses. First, the dried electrospun nanofiber meshes were sliced into small, circular flakes with a diameter of 1 cm. The membranes were then immersed in ethanol/water (9:1) solution containing EDC and NHS for 24 hours at 4°C. The Mol ratio of EDC/NHS was kept constant at 2.5:1. After cross-linking, the excessive EDC and

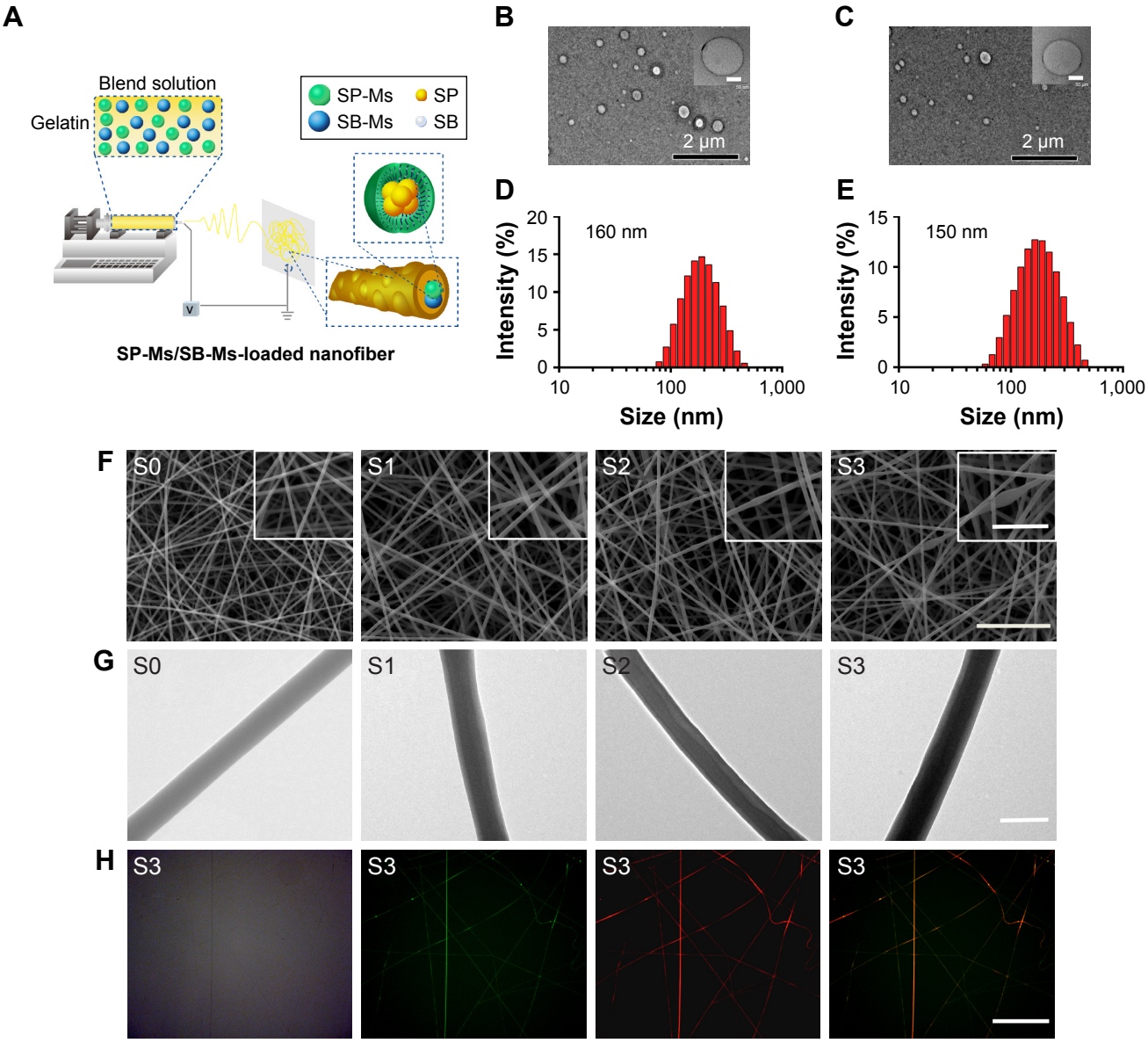

Figure 1 (**A**) Schematic illustrations of the fabrication of the nanoscale dual drug delivery system (SP-Ms/SB-Ms-loaded nanofiber) via electrospinning process. The morphology and size distribution of SP600125-loaded micelles and SB203580-loaded micelles are shown. (**B**) SP600125-loaded micelles TEM image (inset is the magnified image). (**C**) SB203580-loaded micelles TEM image (inset is the magnified image). (**D**, **E**) The corresponding diameter distributions of SP600125-loaded micelles (**D**) and SB203580-loaded micelles (**E**). Scale bar (insets) =50 nm. The morphology and diameter distribution of micelles-loaded composite nanofibers. (**F**) SEM images of S0, S1, S2, and S3 samples (insets are the magnified images). Scale bar =10 μm and the inserts bars =2 μm. (**G**) The corresponding TEM images of S0, S1, S2, and S3 samples. Scale bar =1 μm. (**H**) CLSM images of the electrospun SP600125-Ms/SB203580-Ms nanofibers. The images from left to right show the bright field, emission of the SP600125-Ms-loaded nanofibers, emission of the SB203580-Ms-loaded nanofibers, and an overlaid representation of all components, respectively. Scale bar =50 μm.

Abbreviations: CLSM, confocal laser scanning microcopy; S, solution; SB, SB203580; SB-Ms, SB203580-micelles; SEM, scanning electron microscope; SP, SP600125; SP-Ms, SP600125-micelles; TEM, transmission electron microscope.

NHS were removed by rinsing the membrane thoroughly with 100 mM PBS (pH 7.4), after which the membranes were dried and sterilized with 24 kGy of γ-radiation for 20 hours (China Biotec Co., Taichung, Taiwan).

The release behavior of the different drug-loaded micelles was then studied. Three flakes of samples were placed in meter glass and incubated in 15 mL PBS, and then the samples were kept in a heated incubator and maintained at 37°C and shaken at a speed of 100 cycles·min^{-1}. At pre-set intervals, 1 mL of the release medium outside the dialysis bag was collected and 1 mL of fresh PBS was added in bag. The samples were then collected and subjected to UV spectroscopy at optical wavelengths of 301 nm and 313 nm for SP600125 and SB203580, respectively. The cumulative amounts of drugs were calculated accordingly, and the percentage of the released drugs was plotted against time.

Cell culture

Human periodontal ligament cells (HPDLCs) were taken from healthy, adult premolars extracted for orthodontic reasons. All experimental protocols were conducted in full accordance with ethical principles of the Code of Ethics of the World Medical Association and approved by the Ethics Committee of School of Stomatology, Tongji University, China. Informed consents were obtained before tooth extraction. First, the molars were washed with PBS three times and the PDL tissue was dissected from the mid-third portion of the premolar root with a surgical scalpel. The tissue explants were then placed into a 25 cm^2 culture flask and left upright in a 37°C incubator in 5% CO_2 atmosphere for 30 minutes to allow tissue adhesion. Next, 3 mL of DMEM containing 10% FBS and 1% penicillin/streptomycin was added and the flask was carefully laid down in the incubator. The first media change was conducted after 4 days of post-extraction, and after 1 week of culture, cells began to migrate outward from the PDL tissues until reaching confluence (about 2–3 weeks). The cells were then passaged using 0.25% trypsin and further expanded until P3.

Cells were cultured on the nanofiber scaffolds at a density of 1×10^4 cells/cm^2. At the set time points, CCK-8 solution was added to each well and incubated for 3 hours. The OD of each well at 450 nm was determined with a spectrophotometer (BioTek, Winooski, VT, USA).

Cell imaging

HPDLCs were seeded in a 24-well cell culture plate at a density of 1.5×10^5 cells per sample, and samples with cells on tissue culture polystyrene (TCP) served as control group. After 7 days, we fixed all samples with 4% paraformaldehyde for 10 minutes, washed them three times with PBS, and immersed them in 0.1% Triton-X100 for 10 minutes, and then stained them with FITC-Phalloidin and 4′, 6-diamidino-2-phenylindole. For MMP expression detection, samples were blocked with 10% goat serum for 1 hour at room temperature and incubated in MMP-2 rat-specific primary antibodies at 1:200 dilutions. After further incubation with DyLight 549-conjugated anti-rat IgG antibody at 37°C for 1 hour, the samples were observed under identical conditions by CLSM.

Real-time PCR

To measure MMP expression, we used quantitative real-time PCR (MyiQ™; Bio-Rad, Hercules, CA, USA) according to the manufacturer's protocol. Total RNA was extracted from HPDL fibroblasts by TRIzol Reagent from Thermo Fisher Scientific, and first-strand complementary DNA (cDNA) was synthesized using a PrimeScript first Strand cDNA Synthesis kit (Takara, Tokyo, Japan). The reverse transcription conditions were 45°C for 60 minutes and 95°C for 5 minutes. Real-time PCR was then performed with 20 µL SYBR Premix EX Taq ‖ solution (Takara) containing 10 µmol/L of each of the specific primers, which were designed as listed in Table 2.

Western blot analysis

Protein-level expression was evaluated in the cell culture supernatants of cell-seeded scaffolds 24 hours after 5 µg/mL LPS treatment. We determined protein concentration via Bradford protein assay (Beyotime Biotechnology, Beijing, China). Total protein (25 µg) was loaded on SDS-PAGE, and then transferred to polyvinylidene fluoride membranes (EMD Millipore) which were blocked and cultured at 4°C overnight with the corresponding primary antibodies in blocking solution. Digital images of the chemiluminescence activity were obtained through a digital gel documentation system (Bio-Rad).

Periodontal disease induction

Class II furcation defects were created in the furcation areas of the maxillary and mandibular second and third premolars of four male, 12-month-old beagle dogs. This study was approved by the Animal Ethics Committee of the Second Military Medical University. Written informed consent was performed in accordance with the Institutional Animal Use and Care regulations of the Second Military Medical University. The defects were controlled at the following dimensions: 5 mm apicocoronally, 5 mm mesiodistally, and 3 mm buccolingually. After scaling PDL scales and debris from

Table 2 Primer sequences for qPCR (GAPDH was used as a calibrator)

Gene	Primer sequences	
	Forward (5′–3′)	**Reverse (5′–3′)**
Human MMP-2	TATGGCTTCTGCCCTGAGAC	CACACCACATCTTTCCGTCA
Human MMP-13	GACCCTGGAGCACTCATGTT	CCTCGGAGACTGGTAATGGC
Human GAPDH	CGCTCTCTGCTCCTCCTGTT	CCATGGTGTCTGAGCGATGT

Abbreviations: GAPDH, glyceraldehyde-3-phosphate dehydrogenase; qPCR, quantitative PCR.

defects, an impression material (Impregum Soft™, 3M) was used to completely fill in the defects. The flaps were closed and the impression material was kept for a total of 21 days. Then, impression materials were removed and postoperative radiographs were taken. Furthermore, 2 μg/mL of recombinant BMP-2 (10 μg; R&D Systems Minneapolis, MN, USA) was mixed within S0, S1, S2, and S3 samples before the electrospinning process. In each dog, the defects received one of the following treatments: 1) an untreated defect, 2) S0 group with BMP-2, 3) S1 group with BMP-2, 4) S2 group with BMP-2, and 5) S3 group with BMP-2. All dogs received postoperative treatment with 300 mg/kg of ampicillin sodium for 3 days. Four dogs were sacrificed at 8 weeks after the operation.

Histological procedure

Animals were euthanized with sodium pentobarbital (0.5 mg/kg). Tissue blocks, including teeth and bones, were collected from the premolar regions. These blocks were fixed in 10% buffered formalin for 10 days, and decalcified in formic acid for 4–6 weeks. Serial sections (7 μm) were cut at the mesial-distal plane. All samples were further stained with hematoxylin-eosin for observation by optical microscopy. The newly formed functional fibers were measured by the angular orientation of fibrous ligament tissues.

Microcomputed tomography (micro-CT)

Samples were stacked in a 30 mm holder and scanned using a CT system at 85 kV and 77 μA. After image construction, two-dimensional (2D) images with axial cuts (10 μm thick) of the samples were chosen as the regions of interest (ROI) for analysis (Figure 5E). The ROI top represented the defect's coronal limit corresponding with the cement-enamel (CEJ) line and the ROI bottom was the apical limit defined by a plane 1 mm to defect height so that only new bone was included in the analysis. The buccal limit on the lower half of the defect was set at a 0.5 mm away from the surface of buccal root area. Then, these 2D images were morphed to form a 3D image. Quantification of bone formation (bone volume/total volume, or BV/TV), trabecular number, thickness, and separation were determined by the gray-level distribution.

Statistical analysis

All experiments were performed in triplicate and the results were given as mean ± standard deviation. We performed single-factor ANOVA to determine the statistical significance. Differences were considered statistically significant at a P-value <0.05.

Results and discussion

Encapsulation of SP600125-Ms and SB203580-Ms in gelatin nanofibers

Micelle/drug-loaded nanofiber scaffolds were obtained by encapsulating drug-loaded micelles, and the fabrication process is shown in Figure 1A. Loading contents/encapsulation efficiencies of SP600125 and SB203580 were 1.3%/1.26% and 87.5%/80%, respectively. As shown in Figure 1B–E, the micelles showed a spherical shape with similar average sizes of 160 nm and 150 nm, respectively. Such small sizes indicated that both SP600125-Ms and SB203580-Ms are in favor of being incorporated into polymeric nanofibers.

To confirm the successful loading of micelles into nanofibers, we firstly investigated the structure of nanofiber scaffolds with field-emission SEM (Figure 1F). Pure gelatin nanofibers were uniform in diameter (280±62 nm) and smooth in appearance (sample S0). After introducing SP-Ms and SB-Ms, the nanofiber surfaces (SP-M/SB-M-nanofibers) became rough with obvious spindle-knots (S1, S2, S3) being observed. Under different micelle combinations, the average nanofiber diameters changed slightly (360±62 nm for S1, 343±77 nm for S2, and 358±75 nm for S3). It should be noted here that unlike inorganic nanoparticles, polymeric micelles were hardly identified within nanofibers, due to the lack of contrast between the two polymers. The variation in appearance and average diameter of fibers between pure gelatin nanofibers and micelle-loaded nanofibers implied that these micelles had led to variations in fiber morphology.[25] The content of micelles in the polymer is an important factor, which can affect the morphology of nanofibers. In particular, when the content of micelles was 15%, the surface of composite nanofibers was rough and a lot of protrusions were observed on the surface of nanofibers.[26]

The encapsulation of micelles was demonstrated by TEM. As shown Figure 1G, no core–shell structure was found in the S0 sample, whereas this structure could be easily seen in the micelle-loaded nanofibers (samples S1, S2, and S3). This is due to the fact that the copolymer has much higher crystallinity than gelatin. Moreover, fiber diameter became more widely distributed because of the incorporated micelles, and the micelles exhibited a uniform dispersion in nanofibers. Both SEM and TEM images confirmed that the micelles were successfully loaded into the nanofibers. They also suggested that at the concentration of 8%, the incorporation of micelles into nanofibers had little influence on the formation of nanofibers, and the incorporated contents could be homogenously dispersed into micelles.

CLSM images provided more visualized evidence by showing the distribution of SP-Ms and SB-Ms within gelatin nanofibers (Figure 1H). The encapsulated SP-Ms and SB-Ms were not visible in bright-field mode. SP-Ms emitted green light due to the labeled micelles, which is attributed to the homogenous dispersion of Alexa Fluor 488 NHS Ester, while SB-Ms emitted red light due to the label of Alexa Fluor 647 NHS Ester. The overlaid image demonstrates the successful encapsulation of SP-Ms and SB-Ms within the electrospun nanofibers. In consistent with TEM results, the CLSM images confirmed that both types of the micelles were distributed along fiber axis in a continuous manner. This phenomenon is identical to previous reports, in that nanoparticles were linearly encapsulated by the PCL fibers and formed chainlike structures along the fiber direction.[27]

In vitro drug release study

Derived from partial hydrolysis of native collagen, gelatin has been widely used for pharmaceutical and medical purposes, including wound dressings and drug carriers.[28] Despite the non-toxic and affordable characteristics of gelatin, it is well known that the protein is easily destroyed by water. To prevent rapid dissolution of gelatin during the releasing period, gelatin nanofibers were cross-linked by EDC/NHS. The nanofibers were slightly swelled by EDC/NHS. Figure 2A and B shows the release of SP600125 and SB203580 from the hybrid scaffold during the period of 14 days. We observed same release behavior for SP600125 and SB203580, but the cumulative release of SP600125 was much higher than that of SB203580. Release of both drugs was detected in S3 (52% for SP600125 and 50% for

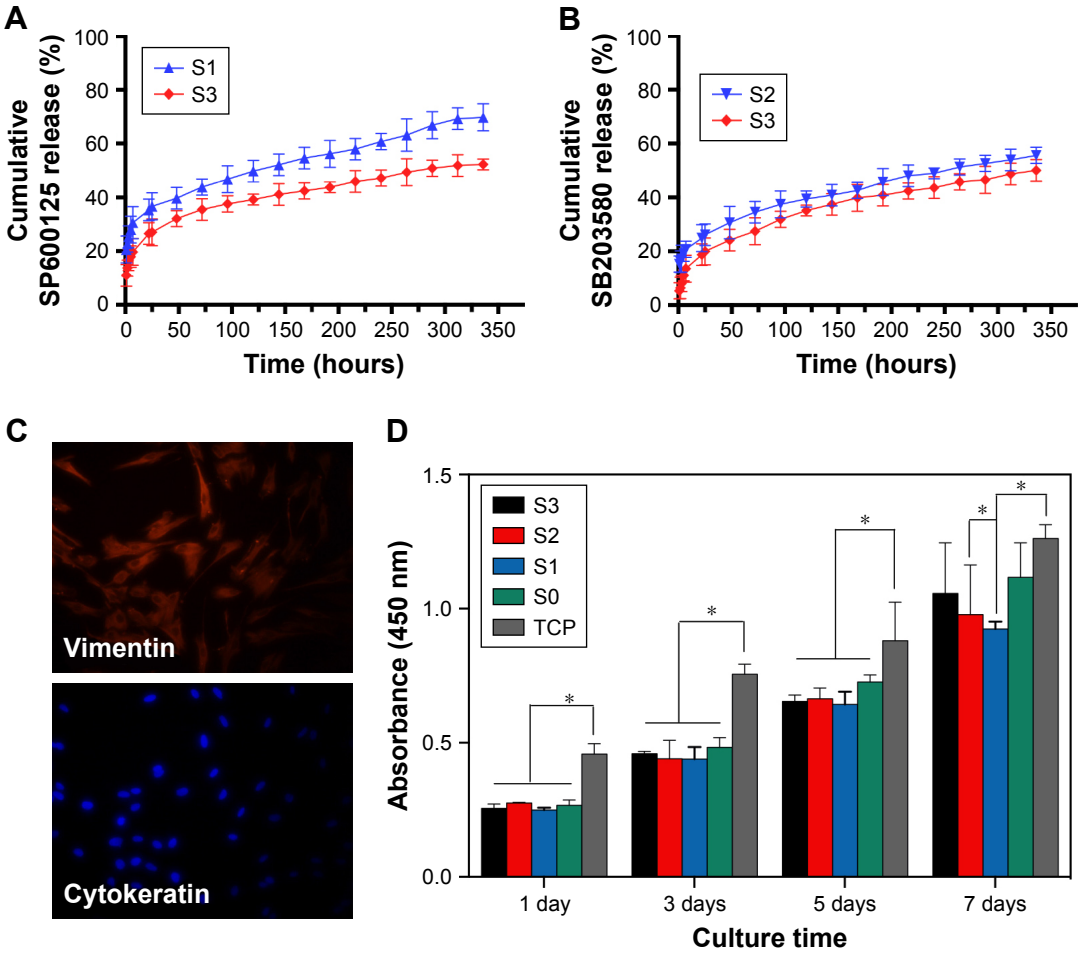

Figure 2 (**A**) Cumulative release profiles of SP600125 from S1 and S3 nanofibrous mats. (**B**) Cumulative release profiles of SB203580 from S2 and S3 nanofibrous mats. (**C**) Identification of cells. Primary cultured human PDL fibroblasts were identified by immunofluorescence staining using antibodies specific for the fibroblast protein maker vimentin and for the epithelial protein maker cytokeratin followed by secondary antibody (red). (**D**) CCK-8 assay of HPDLCs proliferation on S0, S1, S2, S3 scaffolds and on TCP as control after 1, 3, 5, and 7 days of culture. *$P<0.05$ compared to the corresponding controls.

Abbreviations: CCK-8, Cell Counting Kit-8; HPDLCs, human periodontal ligament cells; PDL, periodontal ligament cell; S, solution; TCP, tissue culture polystyrene.

SB203580) sample. When compared to single drug-loaded groups (69% for SP600125 in S1 and 55% for SB203580 in S2), S3 showed the best controlled release rates of all the films, at 52% for SP600125 and 50% for SB203580. Moreover, as shown in Figure 2A, release of SP600125 in S1 was significantly faster than that of S3, and the release rate for SB203580 of S2 was equal to that of S3 (Figure 2B). According to Karolyn's study on dual drug-loaded chitosan carrier (quercetin and 5-fluorouracil [5-FU]),[29] an initial burst release was observed at all pH values for 4 hours due to the release of surface-localized quercetin. The burst release was followed by a phase of sustained release. At pH 5.5, complete release was achieved in 32 hours. At pH 7.4 and 9.2, only about 72% and 68.8% of the drug was released, respectively, at the same time. In the case of 5-FU, an initial burst release that was less than 25% was observed in all cases. As in the case of quercetin, the maximum release of 5-FU was observed at pH 5.5 due to the maximum swelling exhibited at this pH. The release of different drugs from nanoparticles depends on different pH values, and hence it is expected that this property may influence the higher release kinetics of SP600125 (at pH 7.4) than that of SB203580 (at pH 7.4). These results showed that the cumulative release of SP600125 and SB203580 from S3 was optimal, and S3 showed a composite drug release ratio that could effectively enhance drug diffusion. The cross-linking reaction of these composite polymer fibers made the hybrid film more densely packed, which might also impede the drug diffusion. Biodegradable nanoparticles can penetrate into alveolar bone trabeculae, underlying connective tissue, and even the periodontal pocket areas below the gum to target periodontitis.[30,31] As evidenced by the release results, extended MMP inhibition in periodontal pockets can be realized by containing micelles with MMPIs incorporated into electrospun fibers. It is particularly relevant that S3 presented an effective delivery system for SP600125 and SB203580. The electrospun scaffold could not only enhance drug loading, but also improve the permeation ability of periodontal therapy (owning to the extremely small and spherical shape of the nanoparticles). The drug release behavior of S3 also showed that combined drug-loaded nanoparticles incorporated into the scaffold film effectively prolonged the release rate of SP600125 and SB203580.

In vitro toxicity

As shown by the immunofluorescence analysis in Figure 2C, cells showed a strong staining for vimentin, but were negative for cytokeratin, indicating that HPDLCs were from mesenchymal origin. We examined the proliferation of HPDLCs onto the gelatin nanofibers by fluorescence imaging and CCK-8 assay (Figure 2D). On the first 3 days of cell culture, there was a significant increase ($P \leq 0.05$) in cell proliferation on TCP than on nanofiber samples. The reason is that the surface of TCP was coated with a layer of protein to promote cell adhesion, while for other samples, it has been proved that cell adhesion would be hampered by the release of drugs.[32] After 5 days, we still observed a higher increase in cell proliferation on TCP, but the difference between TCP and S0 was lower than that at the first 3 days. After 7 days of culture, no significant difference in the number of cells was found among S0, S3, and TCP, and the cell proliferation on S3 scaffolds was higher than that on S1 and S2 scaffolds. This is probably because that electrospun scaffolds are advantageous for cell proliferation owing to their physical similarity to the natural ECM structure.[33] The cell growth behavior may be in accordance with the drug release profile (Figure 2A and B). After 7 days, higher release kinetics of S1 results in more release of drugs than from other samples. Therefore, S1 may have the most obvious cytotoxicity. Although similar release pattern was observed in S2 and S3, the cumulative release of SB203580 from S2 was much higher than that from S3 because S2 contains 8% SB203580-loaded micelles into a 60% (w/v) gelatin scaffold, while S3 contains 4% SB203580-loaded micelles. S3 reduces the amount of two drugs and therefore shows better cell growth when compared with single drug delivery system.

Samples at 7 days were further stained for fluorescence analysis. As shown in Figure 3, red, blue, and green fluorescence represents the 549-conjugated anti-rat IgG antibody for MMP-2 protein, DAPI-stained cell nuclei, and the Alexa Flour@488 phalloidin-stained actin, respectively. Number of cells increased continuously throughout the culture period. Notably, when phalloidin was used to stain cells on S0, S1, S2, and S3 scaffolds, cell actin was not visible because phalloidin was more easily absorbed by gelatin nanofibers. Similar to the results from CCK-8 assay (Figure 2D), cell density on TCP was considerably higher when compared to that on S0, S1, S2, and S3 scaffolds after 1 day of culture (Figure 3). HPDLCs cultured on S0 and S3 scaffolds also showed faster proliferation than that on S1 and S2 scaffolds, whereas no significant differences in proliferation were found among S0, S3, and TCPs. In addition, the difference in MMP-2 expression was negligible after 1 and 7 days of cell culture, which can be attributed to the fact that Pro-MMP-2 was constitutively expressed in the cells and MMP-2 was barely detected in cell images.

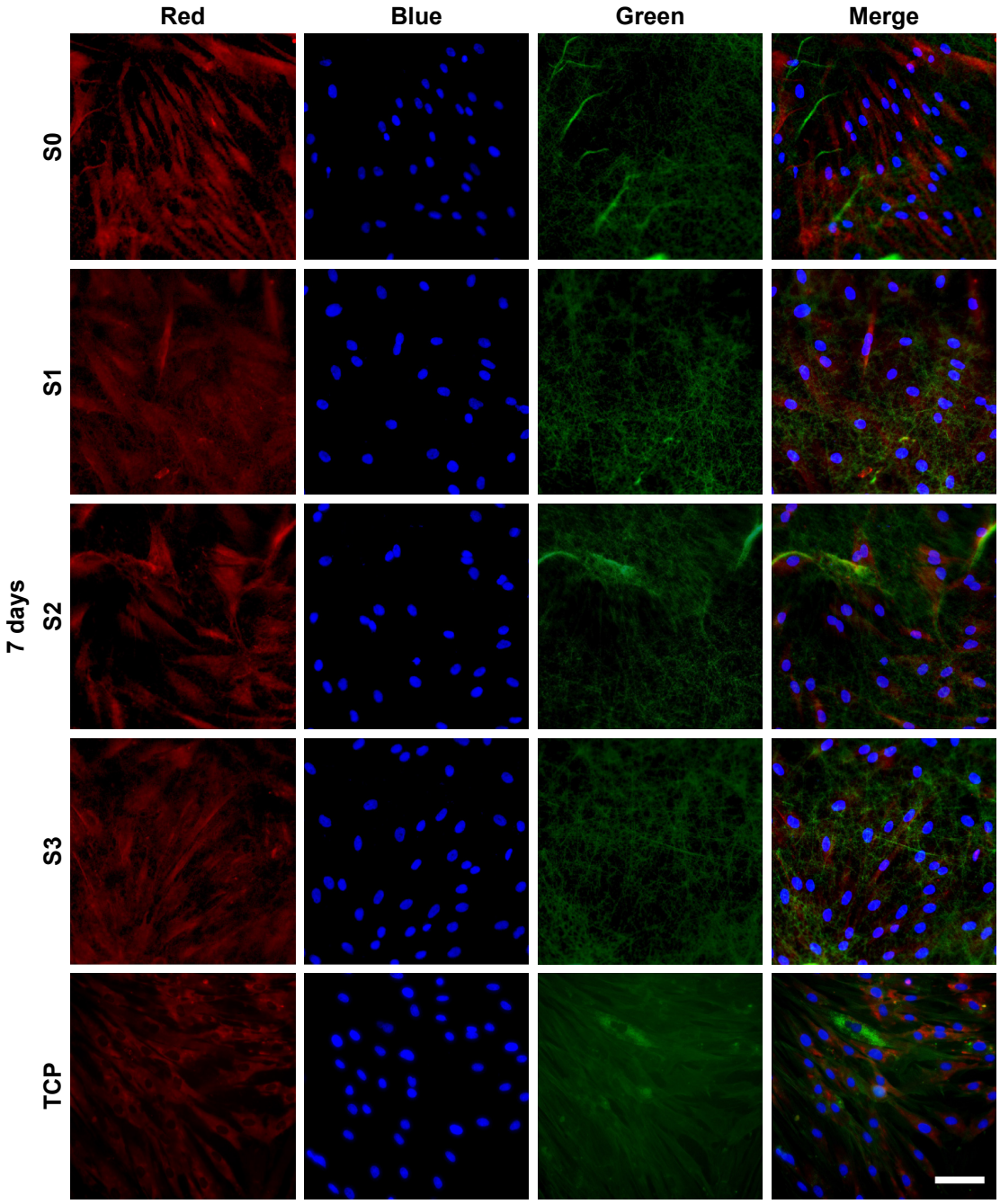

Figure 3 Confocal laser scanning microscopy images of HPDLCs on S0, S1, S2, and S3 scaffolds for 7 days.
Notes: Red, blue, and green fluorescence represent the 549-conjugated anti-rat IgG antibody for MMP-2, DAPI-stained cell nuclei, and the Alexa Flour@488 phalloidin-stained actin, respectively. Scale bar =50 μm.
Abbreviations: HPDLCs, human periodontal ligament cells; S, solution; TCP, tissue culture polystyrene.

Potential of SP-M and SB-M-loaded nanofibers to inhibit expressions of MMP-2, MMP-13

To investigate the potential of SP-Ms and SB-Ms nanofibers in terms of periodontal therapy, we examined the MMP-2 and MMP-13 expression induced by LPS in HPDLCs. Real-time PCR analysis after 8 hours of incubation showed that the mRNA expression of MMP-2 and MMP-13 increased significantly after seeding cells with 5 μg/mL of LPS. We investigated the influence of different concentrations of LPS (varying from 0 to 10 μg/mL) on PDL cells, and the mRNA expression was the strongest at 5 μg/mL (Figure 4A and B). Yan reported that mRNA expression of MMP-1 was strongest at 10 ng/mL IL-17A concentration. Further increase of IL-17A concentration resulted in gradual declines

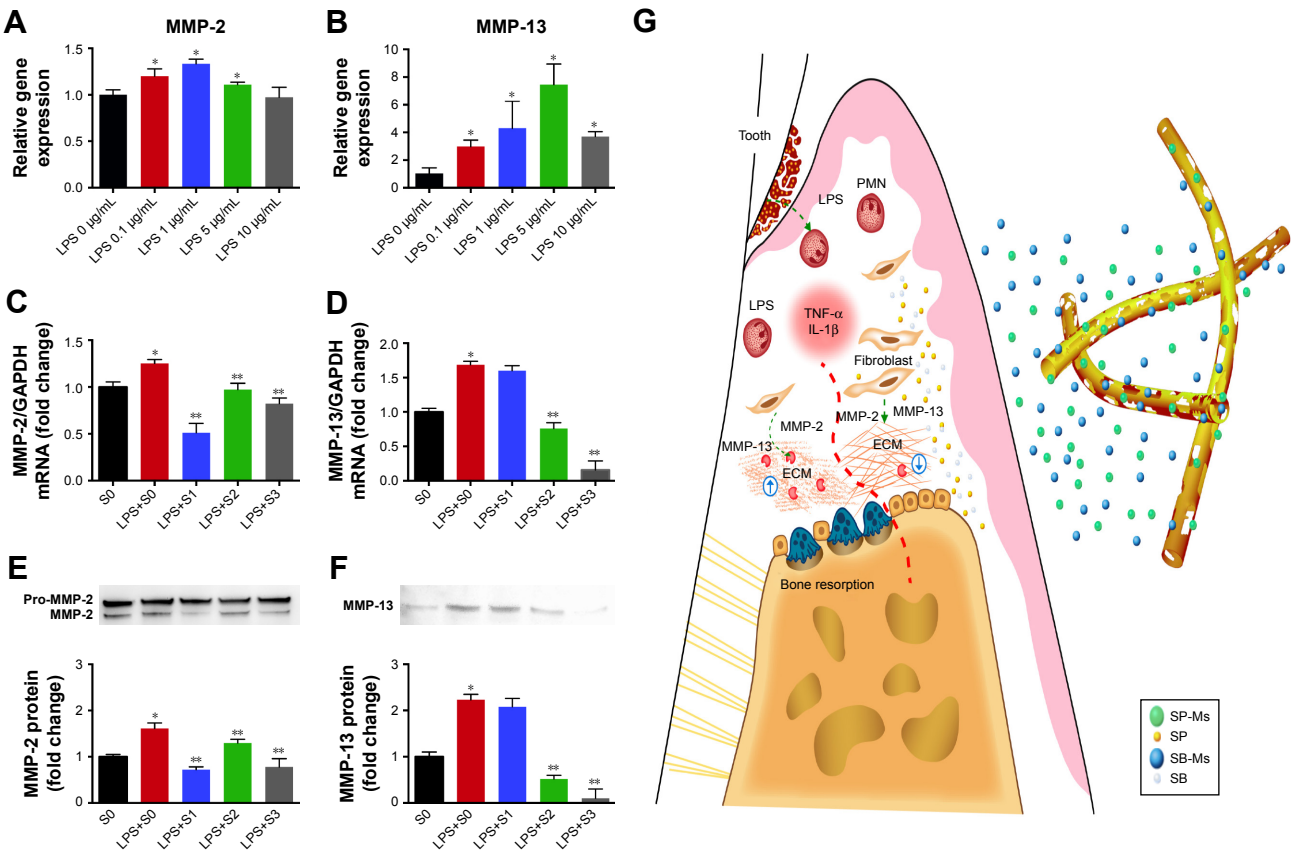

Figure 4 LPS-induced MMP-2 and MMP-13 expression.

Notes: (**A**) Different LPS concentrations induce MMP-2 mRNA. *$P<0.05$, significant difference as compared with the LPS 0 μg/mL. (**B**) Different LPS concentrations induce MMP-13 mRNA. Effects of S0, S1, S2, and S3 scaffolds on the expression MMP-2 and MMP-13 stimulated by LPS (5 μg/mL). (**C**, **D**) Cells were incubated with LPS for 8 hours, and the expression levels of MMP-2 and MMP-13 mRNAs were determined using real-time PCR. (**E**, **F**) Cells were incubated with LPS for 24 hours, and MMP-2 (**E**) and MMP-13 (**F**) protein levels in supernatant were assayed by Western blot. The data represent mean ± SD of three independent experiments. (**G**) Dual drug delivery system (SP-Ms/SB-Ms-loaded nanofiber) regulates matrix degradation and bone resorption in periodontal environment. *$P<0.05$, significant difference as compared with the S0 and **$P<0.05$, significant difference as compared with the LPS+S0.

Abbreviations: ECM, extracelluar matrix; LPS, lipopolysaccharide; PMN, polymorphonuclearleucocyte; S, solution; SB, SB203580; SB-Ms, SB203580-micelles; SP, SP600125; SP-Ms, SP600125-micelles.

in MMP-1 expression.[34] Our results reveal that MMP-2 and MMP-13 expressions are upregulated when LPS is administrated at doses of 1 or 5 μg/mL and then gradually declines at higher doses. These results illustrate the effects of LPS shift in favor of the physiological functions of MMP-2 and MMP-13. As shown in Figure 4C and D, 1 μg/mL of LPS significantly reduced MMP-2 expression, but showed no effect on MMP-13 expression induced by 5 μg/mL of LPS. MMP-2 expression was inhibited by S2, owing to the fact that SP600125 (a JNK inhibitor) has strong effect on MMP-2 but little influence on MMP-13, while SB203580 (a p38 inhibitor) inhibited MMP-2 and MMP-13 expression to a moderate extent. In contrast, S3 inhibited MMP-2 production by 40% and MMP-13 production by >50%, when compared to LPS-induced S0 without drugs. Such results make us believe that SP600125 alone has no effect on MMP-13 gene expression, but the combination of SP600125 (JNK) and SB203580 (p38 MAPK) may pose a synergistic effect.

We also performed Western blotting analysis to determine whether the biochemical inhibitors had been translated to protein level. Cell culture supernatant was harvested after 24 hours of LPS treatment and subjected to analysis. As shown in Figure 4E and F, the conditioned medium from HPDLCs showed bands at 48, 62, and 72 kD, representing the proenzyme form of MMP-2 (Pro-MMP-2), the active form of MMP-2 (MMP-2), and the active form of MMP-13 (MMP-13), respectively. Pro-MMP-2 was expressed constitutively in the HPDLCs, while MMP-2 and MMP-13 were barely detectable. In addition, the protein expression of MMP-2 and MMP-13 increased by ~161% and ~223% after 24 hours of incubation with LPS. We noticed a considerable decrease (by 72% in S1 and 78% in S3) in overall MMP-2 expression (Figure 4E), and a similar decrease (by 52% in S2 and 10% in S3) in MMP-13 expression (Figure 4F). These results were in accordance with the real-time PCR assay, which confirmed together that SP-Ms and SB-Ms nanofibrous scaffolds (S3) could inhibit

MMP-2 and MMP-13 expression in a more effective way than scaffolds containing only one drug.

Polymorphonuclear leukocytes (PMNs) were considered as the first defense line for LPS from Gram-negative plaque biofilms.[35] Monocytes and activated macrophages respond to endotoxins by releasing cytokines (TNF-α and IL-1β) that promote the destructive process, and MMPs are produced by fibroblasts and PMNs. MMPs can denature and degrade collagens and other ECM components. Moreover, recent studies had shown that MMP dysregulation is involved in periodontal ECM remolding development, and that MMPs are responsible for mineralized tissue destruction during bone resorption.[36] As a result, MMPs are considered to be viable drug targets in the therapy of these diseases. Despite the high therapeutic potential of MMPIs, all clinical trials have failed to date, except for doxycycline for periodontal disease.[37] This can be attributed to the poor selectivity of MMPs due to the water-insoluble nature and the poorly defined predictive preclinical animal models for safety and efficacy. As illustrated in Figure 4G, the presence of microbial pathogens in periodontal environments triggers an initial production of proinflammatory cytokines, such as TNF-α and IL-1β, which stimulate the expression and activation of MMPs that degrade extracellular connective tissue matrix. The degradation of connective tissue matrix further leads to the formation of osteoclasts and osteoclast activity. The combined SP-Ms/SB-Ms-loaded nanofibers release SP600125 and SB203580 that may restrain the degradation of connective tissue matrix and subsequently reduce bone resorption when compared with the destructive condition of the left side of the boundary. The micelles system solved the problem of the solubility of the hydrophobic drugs, as the micelles were incorporated into polymeric nanofiber scaffolds. Due to the mimicking of the structure of native ECM and high encapsulation efficiency of micelles, drugs are sustainably released from the scaffolds for a long time to match the growth rate of bone. To our knowledge, this is the first report to show that a dual drug-loaded nanofiber system could be used to suppress both MMP-2 and MMP-13 expression by hydrophobic drugs and can act as an attractive potential target for the treatment of chronic inflammatory bone diseases, such as periodontal diseases.

Histological analysis and micro-CT

Mucoperiosteal flaps were elevated to expose periodontal buccal bone walls (Figure 5A–E). Histological analysis revealed that after 8 weeks of treatment, the defects were partly filled

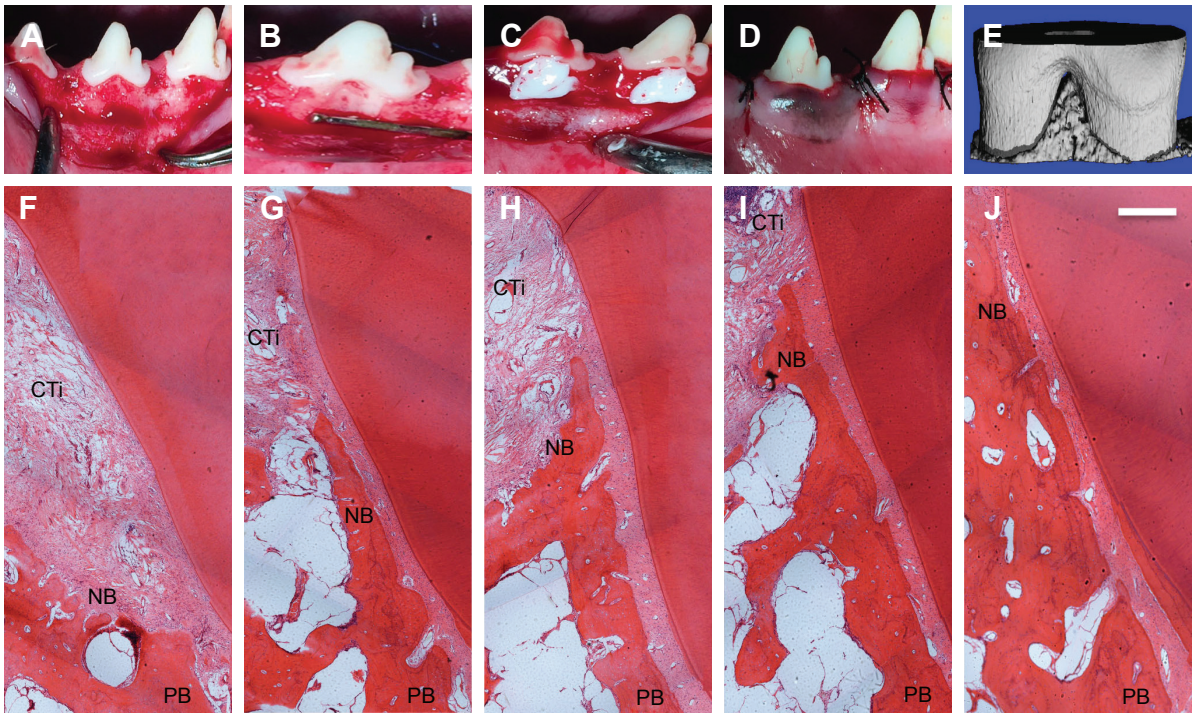

Figure 5 Sequence of in vivo procedures.
Notes: (**A**) Mucoperiosteal flaps were elevated to expose periodontal buccal bone walls. (**B**) The defects were having the following dimensions: 5 mm apicocoronally, 5 mm mesiodistally, and 3 mm buccolingually. (**C**) After scaling periodontal ligament scales and debris from defects, an impression material (Impregum Soft™, 3M) was completely filled in the defects. (**D**) The defects were covered by biomaterials and the mucoperiosteal flaps were restored. (**E**) ROI was used in analysis of alveolar bone. (**F–J**) Histology of bone regeneration in class II furcation defects at 8 weeks. (**F**) The control group. (**G**) The S0 group with BMP-2. (**H**) The S1 group with BMP-2. (**I**) The S2 group with BMP-2. (**J**) The S3 group with BMP-2. Scale bar =500 μm.
Abbreviations: CTi, connective tissue; NB, new bone; PB, pre-existing bone; ROI, region of interest; S, solution.

with alveolar bone. The negative control and S0, S1, S2, and S3 treated groups all demonstrated new alveolar bone, PDL formation, and cementum (Figure 5F–J). These tissues stretched from the pre-existing bone, PDL, and cementum at the base of the defect. The furcation defect was found to be filled with cell-rich connective tissue, especially in the control group. As shown in Figure 5G–J, the amount of cementum was much greater in the S0, S1, S2, and S3 groups than that in the control group, probably owing to the fact that BMP-2 strongly promoted periodontal healing. This result is identical to previous study, in which 40 μg of RhBMP-2 was effective for periodontal regeneration created by experimental periodontitis in beagle dogs.[38] Bone regeneration in S3 group was much more than in control group, indicating that the application of dual drugs had the advantage of controlling the inflammation of bone, and hence promoting the bone regeneration. Furthermore, PDL cell proliferation, gene expression, osteogenic differentiation, and mineralization have all been regulated via MAPK pathway, especially p38 MAPK and JNK pathways. There was also obvious difference between S3 and other drug-loaded groups, because after the long-term release period, MMPIs have been released totally. In accordance to in vitro drug release results, after 14 days, S3 showed the best overall release of all samples (52% for SP600125 and 50% for SB203580), when compared to 69% for SP600125 in S1 and 55% for SB203580 in S2. To quantitatively evaluate fiber formation and orientation of PDL, the angles of fiber bundles against the root surface are marked in Figure 6A–E. Compared with the angulation of fibers in control group, S3 group demonstrated largest angulation, and there was no obvious

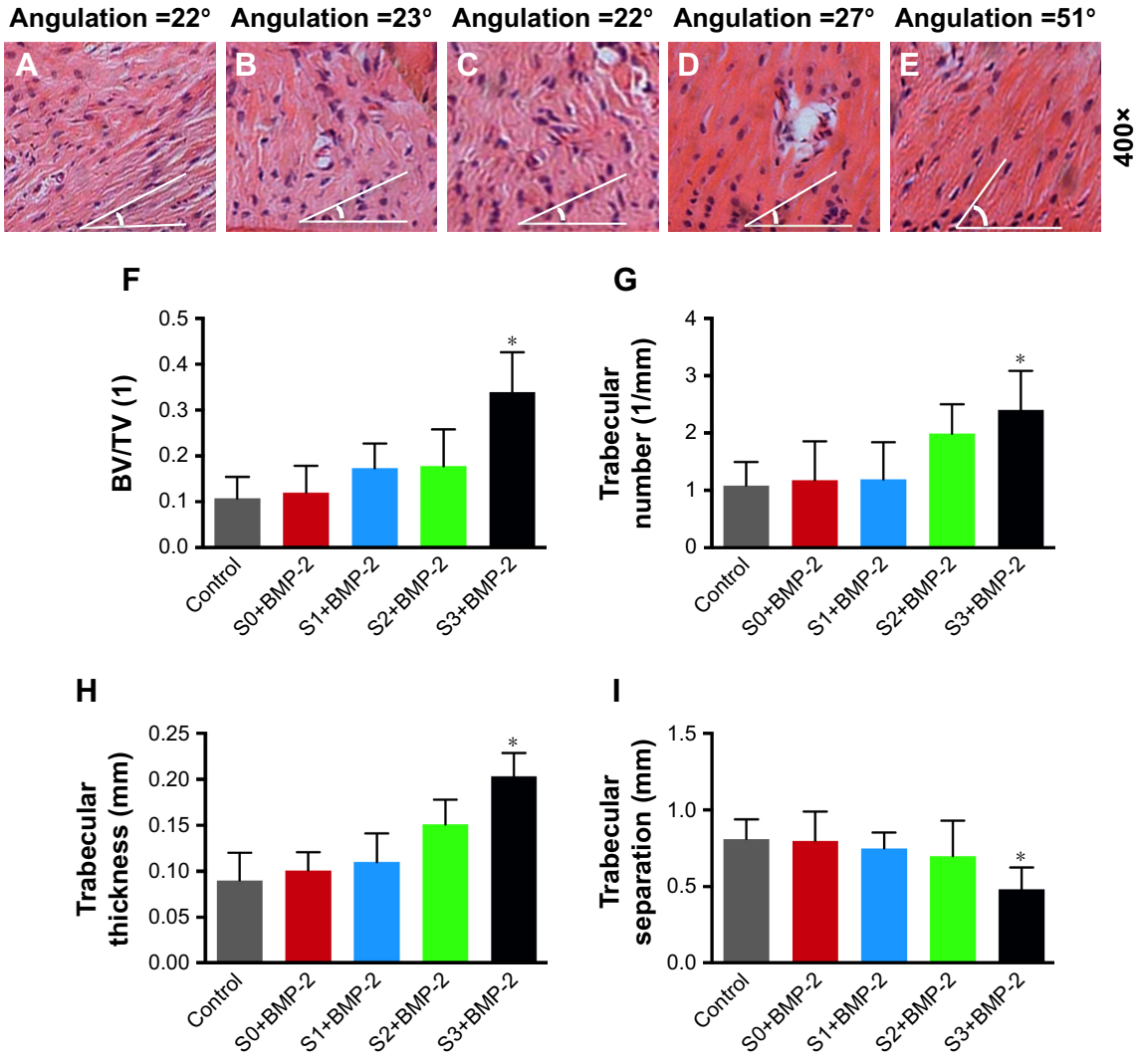

Figure 6 Histology of the periodontal defects at 8 weeks post-surgery.
Notes: (**A**–**E**) The angle represents the angulation of regenerated ligament direction of each representative image: (**A**) the control group, (**B**) the S0 group with BMP-2, (**C**) the S1 group with BMP-2, (**D**) the S2 group with BMP-2, and (**E**) the S3 group with BMP-2. Scale bar =50 μm. (**F**–**I**) Micro-CT images: (**F**) bone volume per total volume (BV/TV), (**G**) trabecular number, (**H**) trabecular thickness, and (**I**) trabecular separation of various groups. *$P<0.05$ compared with control.
Abbreviations: Micro-CT, microcomputed tomography; S, solution.

difference in angulation between control and S0, S1, and S2 groups. These results inferred that S3 group might better guide ligament orientation. As shown by the 3D images of defect area (Figure 6F–I), micro-CT volumetric values showed more bone volume per total volume in S3-treated group than in the control group at 8 weeks. Also, the trabecular number and thickness of S3-treated group were significantly higher and trabeculae separation was lower than those of control group at 8 weeks (Figure 6G–I). Kosen fabricated collagen hydrogel/sponge scaffold facilitating periodontal wound healing in class II furcation in beagle dogs. At 4 weeks, reconstruction of alveolar bone and cementum was frequently observed after surgery. PDL tissue was also re-established between alveolar bone and cementum.[39] Previous study reported that recombinant human basic fibroblast growth factor (bFGF) stimulates periodontal regeneration in class II furcation defects created in beagle dogs. At 6 weeks, in all sites where bFGF was applied, PDL formation with new cementum deposits and new bone formation was observed histomorphometrically. It exhibited significant regeneration by the new bone formation rate (83.6%±14.3%).[40] The present results indicate that an 8-week period is long enough for beagle dogs to reach being partly filled with alveolar bone. In our study, S3 group with BMP-2 formed more new bones in a faster manner than other groups, especially after 8 weeks. Also as reported by Sculean et al, the guided tissue regeneration membranes must function for at least 4–6 weeks to allow successful regeneration of the periodontal system.[41] Thus, our dual drug delivery system can be considered as a biodegradable membrane, providing a protective environment for controlling early inflammation by MMPIs, and eventually confines the effect of BMP-2 favoring periodontal tissue growth within the defect. Although different complex membranes have been developed to favor periodontal regeneration, they usually focused on traditional water-soluble drugs or growth factors in the periodontal regeneration, but experimental work and clinical trials have clearly shown that a lack of control in MMP expression may have lead to impaired bone regeneration of periodontal tissue.[42] In the study, we found more periodontal tissue regeneration at 8 weeks. The results demonstrated that our dual drug delivery system has a synergistic effect of inhibiting the degradation of extracellular connective tissue matrix and promoting bone regeneration than when using only a single inhibitor. In the future, we will further investigate into the in-depth healing mechanism underlying dual drug delivery system and single drug release system.

Conclusion

In summary, we successfully prepared a novel, multi-agent delivery scaffolds for periodontal treatment. The successful encapsulation of SP600125 and SB203580 in polymeric micelles and the subsequent incorporation of these micelles into gelatin nanofibers enabled the release of both drugs to be prolonged effectively. CCK-8 assay implied no cytotoxicity during the release period. Real-time PCR and Western blotting further revealed that the multi-agent delivery system effectively reduced periodontal inflammatory stimuli and increased periodontal regeneration in class II furcation defects. Compared with previous method, our drug-loaded nanofiber ensures the effective concentration of drugs in a restricted area, thereby representing a promising path to the therapy of periodontal disease.

Acknowledgments

We are thankful for the financial support from the National Natural Science Foundation of China (81873715 and 81572114), the Innovation Program of Shanghai Municipal Education Commission (17140903600), and the "Chen Guang" Project sponsored by Shanghai Municipal Education Commission and Shanghai Education Development Foundation (14CG34). An abstract of this paper was presented at the 4th Symposium on Innovative Polymers for Controlled Delivery Conference as a poster presentation talk with interim findings. The poster's abstract has been published.[43]

Disclosure

The authors report no conflicts of interest in this work.

References

1. Amid R, Kadkhodazadeh M, Fekrazad R, Hajizadeh F, Ghafoori A. Comparison of the effect of hand instruments, an ultrasonic scaler, and an erbium-doped yttrium aluminium garnet laser on root surface roughness of teeth with periodontitis: a profilometer study. *J Periodontal Implant Sci*. 2013;43(2):101–105.
2. Apatzidou DA, Kinane DF. Nonsurgical mechanical treatment strategies for periodontal disease. *Dent Clin North Am*. 2010;54(1):1–12.
3. Sapna G, Gokul S, Bagri-Manjrekar K. Matrix metalloproteinases and periodontal diseases. *Oral Dis*. 2014;20(6):538–550.
4. Amălinei C, Căruntu ID, Giuşcă SE, Bălan RA. Matrix metalloproteinases involvement in pathologic conditions. *Rom J Morphol Embryol*. 2010;51(2):215–228.
5. Zitka O, Kukacka J, Krizkova S, et al. Matrix metalloproteinases. *Curr Med Chem*. 2010;17(31):3751–3768.
6. Sapna G, Gokul S, Bagri-Manjrekar K. Matrix metalloproteinases and periodontal diseases. *Oral Dis*. 2014;20(6):538–550.
7. Marcaccini AM, Meschiari CA, Zuardi LR, et al. Gingival crevicular fluid levels of MMP-8, MMP-9, TIMP-2, and MPO decrease after periodontal therapy. *J Clin Periodontol*. 2010;37(2):180–190.
8. Jang YJ, Kim ME, Ko SY. n-Butanol extracts of Panax notoginseng suppress LPS-induced MMP-2 expression in periodontal ligament fibroblasts and inhibit osteoclastogenesis by suppressing MAPK in LPS-activated RAW264.7 cells. *Arch Oral Biol*. 2011;56(11):1319–1327.
9. Caton J, Ryan ME. Clinical studies on the management of periodontal diseases utilizing subantimicrobial dose doxycycline (SDD). *Pharmacol Res*. 2011;63(2):114–120.

10. Shindo S, Hosokawa Y, Hosokawa I, Ozaki K, Matsuo T. Genipin inhibits MMP-1 and MMP-3 release from TNF-a-stimulated human periodontal ligament cells. *Biochimie*. 2014;107 Pt B:391–395.
11. Gao A, Kantarci A, Herrera BS, Gao H, van Dyke TE. A critical role for suppressors of cytokine signaling 3 in regulating LPS-induced transcriptional activation of matrix metalloproteinase-13 in osteoblasts. *PeerJ*. 2013;1(Suppl 2):e51.
12. Mo G, Hu X, Liu S, et al. Influence of coupling bonds on the anti-tumor activity of polymer-pirarubicin conjugates. *Eur J Pharm Sci*. 2012; 46(5):329–335.
13. Yao W, Xu P, Pang Z, et al. Local delivery of minocycline-loaded PEG-PLA nanoparticles for the enhanced treatment of periodontitis in dogs. *Int J Nanomedicine*. 2014;9:3963.
14. Cagel M, Tesan FC, Bernabeu E, et al. Polymeric mixed micelles as nanomedicines: Achievements and perspectives. *Eur J Pharm Biopharm*. 2017;113:211–228.
15. Wei L, Cai C, Lin J, Chen T. Dual-drug delivery system based on hydrogel/micelle composites. *Biomaterials*. 2009;30(13):2606–2613.
16. Amano Y, Ota M, Sekiguchi K, Shibukawa Y, Yamada S. Evaluation of a poly-l-lactic acid membrane and membrane fixing pin for guided tissue regeneration on bone defects in dogs. *Oral Surg Oral Med Oral Pathol Oral Radiol Endod*. 2004;97(2):155–163.
17. Chang C-Y, Yamada S. Evaluation of the regenerative effect of a 25% doxycycline-loaded biodegradable membrane for guided tissue regeneration. *Journal of Periodontology*. 2000;71(7):1086–1093.
18. Roriz VM, Souza SL, Taba M, Palioto DB, Grisi MF. Treatment of Class III furcation defects with expanded polytetrafluoroethylene membrane associated or not with anorganic bone matrix/synthetic cell-binding peptide: a histologic and histomorphometric study in dogs. *J Periodontol*. 2006;77(3):490–497.
19. Rosetti EP, Marcantonio RA, Cirelli JA, Zuza EP, Marcantonio E. Treatment of gingival recession with collagen membrane and DFDBA: a histometric study in dogs. *Braz Oral Res*. 2009;23(3):307–312.
20. Zhang YZ, Su B, Venugopal J, Ramakrishna S, Lim CT. Biomimetic and bioactive nanofibrous scaffolds from electrospun composite nanofibers. *Int J Nanomedicine*. 2007;2(4):623–638.
21. Wang Z, Lin M, Xie Q, et al. Electrospun silk fibroin/poly(lactide-co-ε-caprolactone) nanofibrous scaffolds for bone regeneration. *Int J Nanomedicine*. 2016;11:1483–1500.
22. Bottino MC, Thomas V, Janowski GM. A novel spatially designed and functionally graded electrospun membrane for periodontal regeneration. *Acta Biomater*. 2011;7(1):216–224.
23. Chen X, Liu Y, Miao L, et al. Controlled release of recombinant human cementum protein 1 from electrospun multiphasic scaffold for cementum regeneration. *Int J Nanomedicine*. 2016;11:3145–3158.
24. Ranjbar-Mohammadi M, Zamani M, Prabhakaran MP, Bahrami SH, Ramakrishna S. Electrospinning of PLGA/gum tragacanth nanofibers containing tetracycline hydrochloride for periodontal regeneration. *Materials Science and Engineering: C*. 2016;58:521–531.
25. Liu X, He J. Hierarchically structured superhydrophilic coatings fabricated by self-assembling raspberry-like silica nanospheres. *J Colloid Interface Sci*. 2007;314(1):341–345.
26. Qiu K, He C, Feng W, et al. Doxorubicin-loaded electrospun poly(l-lactic acid)/mesoporous silica nanoparticles composite nanofibers for potential postsurgical cancer treatment. *Journal of Materials Chemistry B*. 2013;1(36):4601–4611.
27. Hu J, Zeng F, Wei J, Chen Y, Chen Y. Novel controlled drug delivery system for multiple drugs based on electrospun nanofibers containing nanomicelles. *Journal of Biomaterials Science, Polymer Edition*. 2014;25(3):257–268.
28. Meng ZX, Xu XX, Zheng W, et al. Preparation and characterization of electrospun PLGA/gelatin nanofibers as a potential drug delivery system. *Colloids and Surfaces B: Biointerfaces*. 2011;84(1):97–102.
29. David KI, Jaidev LR, Sethuraman S, Krishnan UM. Dual drug loaded chitosan nanoparticles – sugar-coated arsenal against pancreatic cancer. *Colloids and Surfaces B: Biointerfaces*. 2015;135:689–698.
30. Zupancic S, Kocbek P, Baumgartner S, Kristl J. Contribution of nanotechnology to improved treatment of periodontal disease. *Curr Pharm Des*. 2015;21(22):3257–3271.
31. Piñón-Segundo E, Ganem-Quintanar A, Alonso-Pérez V, Quintanar-Guerrero D. Preparation and characterization of triclosan nanoparticles for periodontal treatment. *Int J Pharm*. 2005;294(1–2):217–232.
32. Xue J, He M, Liu H, et al. Drug loaded homogeneous electrospun PCL/gelatin hybrid nanofiber structures for anti-infective tissue regeneration membranes. *Biomaterials*. 2014;35(34):9395–9405.
33. Wang X, Ding B, Li B. Biomimetic electrospun nanofibrous structures for tissue engineering. *Mater Today*. 2013;16(6):229–241.
34. Wu Y, Zhu L, Liu L, Zhang J, Peng B. Interleukin-17A stimulates migration of periodontal ligament fibroblasts via p38 MAPK/NF-κB-dependent MMP-1 expression. *J Cell Physiol*. 2014;229(3):292–299.
35. Dixon DR, Darveau RP. Lipopolysaccharide heterogeneity: innate host responses to bacterial modification of lipid a structure. *J Dent Res*. 2005; 84(7):584–595.
36. Woodward JK, Holen I, Coleman RE, Buttle DJ. The roles of proteolytic enzymes in the development of tumour-induced bone disease in breast and prostate cancer. *Bone*. 2007;41(6):912–927.
37. Payne JB, Golub LM, Stoner JA, et al. The effect of subantimicrobial-dose-doxycycline periodontal therapy on serum biomarkers of systemic inflammation: a randomized, double-masked, placebo-controlled clinical trial. *J Am Dent Assoc*. 2011;142(3):262–273.
38. Kinoshita A, Oda S, Takahashi K, Yokota S, Ishikawa I. Periodontal regeneration by application of recombinant human bone morphogenetic protein-2 to horizontal circumferential defects created by experimental periodontitis in beagle dogs. *J Periodontol*. 1997;68(2):103–109.
39. Kosen Y, Miyaji H, Kato A, Sugaya T, Kawanami M. Application of collagen hydrogel/sponge scaffold facilitates periodontal wound healing in class II furcation defects in beagle dogs. *J Periodontal Res*. 2012; 47(5):626–634.
40. Murakami S, Takayama S, Kitamura M, et al. Recombinant human basic fibroblast growth factor (bFGF) stimulates periodontal regeneration in class II furcation defects created in beagle dogs. *J Periodontal Res*. 2003;38(1):97–103.
41. Sculean A, Nikolidakis D, Schwarz F. Regeneration of periodontal tissues: combinations of barrier membranes and grafting materials – biological foundation and preclinical evidence: A systematic review. *Journal of Clinical Periodontology*. 2008;35(Suppl. 3):106–116.
42. Paiva KBS, Granjeiro JM. Bone tissue remodeling and development: Focus on matrix metalloproteinase functions. *Archives of Biochemistry and Biophysics*. 2014;561:74–87.
43. Dual micelles loaded gelatin nanofibers and their application in lipopolysaccharide-induced periodontal disease. *Journal of Controlled Release*. 2017;259:e163.